PHYSICAL REVIEW E **90**, 062302 (2014)

Absence of red structural color in photonic glasses, bird feathers, and certain beetles

Sofia Magkiriadou,[1] Jin-Gyu Park,[2] Young-Seok Kim,[3] and Vinothan N. Manoharan[2,1,*]

[1]*Department of Physics, Harvard University, 17 Oxford Street, Cambridge, Massachusetts 02138*

[2]*School of Engineering and Applied Sciences, Harvard University, 29 Oxford Street, Cambridge, Massachusetts 02138*

[3]*Korea Electronics Technology Institute, Bundang-gu, Seongnam-Si, Gyeonggi-do, Korea*

(Received 30 September 2014; published 3 December 2014)

Colloidal glasses, bird feathers, and beetle scales can all show structural colors arising from short-ranged spatial correlations between scattering centers. Unlike the structural colors arising from Bragg diffraction in ordered materials like opals, the colors of these photonic glasses are independent of orientation, owing to their disordered, isotropic microstructures. However, there are few examples of photonic glasses with angle-independent red colors in nature, and colloidal glasses with particle sizes chosen to yield structural colors in the red show weak color saturation. Using scattering theory, we show that the absence of angle-independent red color can be explained by the tendency of individual particles to backscatter light more strongly in the blue. We discuss how the backscattering resonances of individual particles arise from cavity-like modes and how they interact with the structural resonances to prevent red. Finally, we use the model to develop design rules for colloidal glasses with red, angle-independent structural colors.

DOI: 10.1103/PhysRevE.90.062302 PACS number(s): 82.70.Dd, 78.67.Pt, 42.25.Fx, 42.25.Dd

I. INTRODUCTION

Structural color in materials arises from interference of light scattered from inhomogeneities spaced at scales comparable to optical wavelengths. Opals and most other familiar examples of structurally colored materials are ordered [1,2], and as a result, the color of these photonic crystals [3] depends on their orientation relative to the incident light: they are iridescent. There is another, less well-studied class of materials with angle-independent structural colors. These are called *photonic glasses* [4–7], because the inhomogeneities form a random, glassy arrangement with short-ranged order but no long-ranged order. As in crystals, the average spacing between neighboring scatterers in a photonic glass is narrowly distributed and determines the resonantly scattered wavelength [8,9]. But unlike crystals, photonic glasses are isotropic, so that the condition for constructive interference is independent of orientation. This coloration mechanism is common in the feathers of birds [9–11], whose colors are visually indistinguishable from those of conventional absorbing dyes. Photonic glasses with structural colors in the visible have also been produced in a variety of synthetic colloidal systems [8,12–20].

However, to our knowledge there are no photonic glasses with saturated yellow, orange, or red color. While systems with angle-independent structural red have been reported [12,15,17,18,21], the color saturation for long-wavelength hues is poor compared to that for blue. Interestingly, red angle-independent structural color also appears to be rare in nature. Birds use structural color only for blue and green; red colors in bird feathers come from absorbing pigments [11]. And while the scales of the longhorn beetle *Anoplophora graafi* have structural colors that span the visible spectrum, there are no saturated red colors—only a pale purple [22].

The absence of red photonic glasses does not appear to have been acknowledged, let alone explained. Previous work on photonic glasses [8,9,22–25] has focused on structures found in nature and their biomimetic analogues, nearly all of which are blue. Noh and coworkers [26,27] proposed a theoretical model based on single and double scattering to explain the optical properties of these blue samples, and Liew and coworkers [23] and Rojas-Ochoa and coworkers [5] showed that the interscatterer correlations not only give rise to color but also suppress multiple scattering. However, if the color were entirely determined by correlations, one would expect that all colors could be made simply by linearly rescaling the structure. As we show below, this approach does not work (Fig. 1).

Here we present a model that explains the absence of long-wavelength structural colors in photonic glasses. Our model accounts for both interparticle correlations as well as the scattering behavior of individual particles. We show that short-wavelength resonances in the single-particle scattering cross-section near backscattering introduce a blue peak in the spectrum that changes the hue of a red structural color to purple. These resonances are not the traditional Mie resonances, which occur in the total scattering cross-section, but rather are akin to cavity resonances. The model, which agrees with measured spectra from synthetic photonic glasses, provides a framework for understanding the limitations of current photonic glasses and enables the design of new systems without those limitations.

II. EXPERIMENT

To demonstrate that resonant scattering from the interparticle correlations is not sufficient to explain the colors of photonic glasses, we prepare colloidal glasses from poly(methyl methacrylate) (PMMA) spheres of various diameters and study their colors with spectrometry. Figure 1 shows color photographs and reflection spectra of samples prepared in the same way using three different particle diameters $d = 170$, 240, and 330 nm. These samples were prepared by mixing one part of an aqueous suspension containing 1% w/w carbon black (Cabot) and 2% w/w Pluronic F108 (BASF) with two parts of a monodisperse suspension of PMMA particles at 20% w/w,

*Corresponding author: vnm@seas.harvard.edu

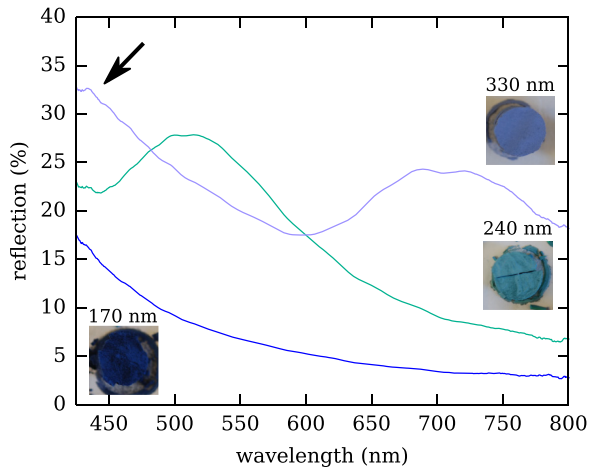

FIG. 1. (Color online) Measured reflectivity spectra for three similarly prepared colloidal glasses of PMMA particles in air. Insets show photographs of the samples and diameters of the particles used to make the samples. The purple sample would appear red if not for the high reflectivity in the blue, indicated by the arrow.

centrifuging the mixture at 5200 g for 30 min, removing the supernatant, and slip-casting on a gypsum substrate. The final samples are amorphous, dense packings of particles in air. The small amount of carbon black suppresses multiple scattering, making it easier to see the color [8].

We measure the reflection spectra as a function of wavelength with a fiber-optic spectrometer (OceanOptics HR2000+) mounted on an optical microscope (Nikon LV-100). The samples are illuminated with white light from a halogen lamp that is collimated by minimizing the condenser aperture. The divergence angle of the beam is 0.02 radians. The light scattered by the sample is collected by a 50× objective (Nikon LU Plan Fluor, NA = 0.8) and imaged onto the detection fiber (OceanOptics QP600-2-UV/VIS). Because the objective NA is the limiting numerical aperture in our system, our measurements include light scattered up to a maximum angle $\theta_{\max} = \arcsin(0.80) = 0.93$ radians. We normalize all spectra to the reflected intensity from an aluminum mirror, average the spectra measured over five different locations on the sample, and then smooth the spectra using a 50-nm window.

Two peaks are visible in the spectra, one at 515 nm in the $d = 240$-nm sample and the other at 710 nm in the $d = 330$-nm sample. The ratio of these peak wavelengths is approximately that of the two particle sizes $330/240 \approx 710/515$. The linear scaling is consistent with the hypothesis that the color is due to constructive interference of light scattered from correlated regions of particles. The high reflectivity of the $d = 170$-nm sample at short wavelengths suggests a structural resonance in the ultraviolet (UV), again consistent with this hypothesis. Thus, the peak wavelength does appear to scale linearly with the particle size, and hence with the lengthscale of structural correlations, assuming that the volume fraction and structure of all of our samples are similar.

However, whereas the $d = 170$-nm sample appears blue and the $d = 240$-nm sample appears green, the $d = 330$-nm sample does not appear red. The reason is that its reflectivity rises toward the blue, suggesting a second peak at 430 nm or below. We have observed similar spectra in samples made of polystyrene and silica particles whenever the particle size is 250 nm or larger. Dong and coworkers [22] found a similarly shaped spectrum, with one peak in the red and another apparent one at short wavelengths, for purple longhorn beetle scales.[1] Takeoka and coworkers [20] also observed a short-wavelength peak in the spectrum of their amorphous packings of $d = 360$-nm silica particles.[2] In order to understand the absence of red in all of these photonic glasses, we must understand the origin of this short-wavelength reflectivity peak.

III. THEORY

To explain our observations, we use a single-scattering model where we treat scattering from a particle assembly as the result of two separable processes: scattering from each individual particle, as described by a form factor, and interference between waves scattered from the particles, as described by the structure factor of the glass. This type of single-scattering model has been used to describe the optical properties of similar systems [5,28]. In our analysis, we first use the form and structure factor to calculate the differential scattering cross-section of a glass, and then we derive a formula that relates this cross-section to reflectivity, the quantity that we measure. According to our model, structural color in photonic glasses is primarily determined by the peaks of the structure factor. As we shall show, the form factor can either undermine this color or enhance it, depending on the structure of the system and the particle properties.

The scattering geometry that we model mimics a typical experimental setup, as shown in Fig. 2. A colloidal glass is illuminated by incident light with wavevector $\mathbf{k}_{\text{in}}$ and scatters light with wavevector $\mathbf{k}_{\text{s}}$. The angle between $\mathbf{k}_{\text{in}}$ and $\mathbf{k}_{\text{s}}$ is θ. The vector difference $\mathbf{q} = \mathbf{k}_{\text{s}} - \mathbf{k}_{\text{in}}$ describes the momentum change between the incident and the scattered wave. The source can emit light into a range of angles defined by the source numerical aperture $\text{NA}_{\text{source}} = \sin(\theta_{\text{s}})$, and the detector can detect light coming from a range of angles defined by the detector numerical aperture $\text{NA}_{\text{detector}} = \sin(\theta_{\text{d}})$.

We assume elastic scattering, so that $|\mathbf{k}_{\text{in}}| = |\mathbf{k}_{\text{s}}| = k = 2\pi n_{\text{eff}}/\lambda$, and

$$q = 2k \sin(\theta/2). \tag{1}$$

Here n_{eff} is the effective refractive index of the medium and λ is the wavelength of light in vacuum. The effective index is a weighted average calculated using the Maxwell-Garnett mean-field approximation [29]:

$$n_{\text{eff}} = n_{\text{med}} \sqrt{\frac{2n_{\text{med}}^2 + n_{\text{p}}^2 + 2\phi\left(n_{\text{p}}^2 - n_{\text{med}}^2\right)}{2n_{\text{med}}^2 + n_{\text{p}}^2 - \phi\left(n_{\text{p}}^2 - n_{\text{med}}^2\right)}}, \tag{2}$$

where n_{med} is the refractive index of the material surrounding the particles (air, in our case), n_{p} is the refractive index of the particles, and ϕ is the volume fraction occupied by the particles. We use the effective index because the particle packings are dense, so that the scattered fields "see" an index intermediate between the particle and medium index. Although

[1] See the bottom spectrum in Fig. 1(c) of Ref. [22].
[2] See the pink curve in Fig. 1(b) of Ref. [20].

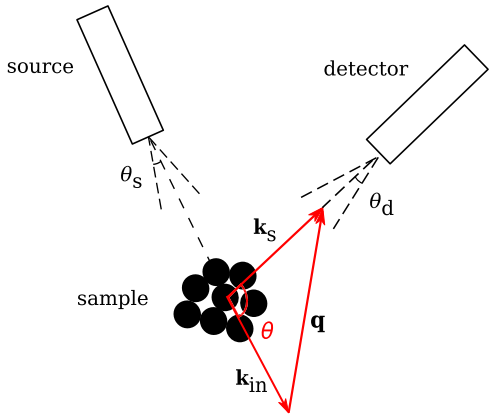

FIG. 2. (Color online) Scattering geometry for our model.

the Maxwell-Garnett approximation is typically used when the refractive index variations are much smaller than the wavelength, Vos and coworkers [30] showed that it is a good approximation even for photonic crystals, and Forster and coworkers [8] have shown the same for photonic glasses.

Assuming perfect monodispersity, we can express the differential scattering cross-section of a glassy ensemble of particles, $d\sigma_{\text{glass}}/d\Omega$, as a product of the form factor F and the structure factor S [5,28]:

$$d\sigma_{\text{glass}}/d\Omega = (1/k^2)FS. \tag{3}$$

The form factor is related to the differential scattering cross-section of a single particle, $d\sigma/d\Omega$, through $F = (1/k^2)d\sigma/d\Omega$ [31]; we calculate F using Mie theory [31,32]. The structure factor is the Fourier transform of the pair correlation function of the particles [33]; we calculate it using a solution to the Ornstein-Zernike equation with the Percus-Yevick closure approximation [34]. In so doing, we are assuming that the structure of our particle glasses is close to that of a hard-sphere liquid. Figure 3 shows S calculated for a volume fraction $\phi = 0.55$ as a function of a dimensionless

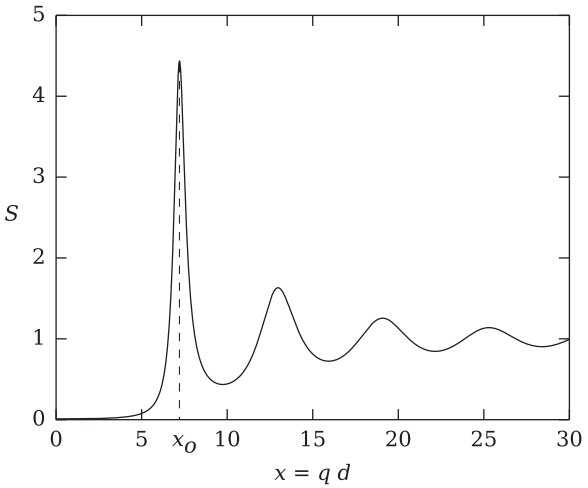

FIG. 3. Structure factor of a colloidal glass with volume fraction $\phi = 0.55$ calculated from the Ornstein-Zernike equation under the Percus-Yevick approximation.

wavevector $x = qd$, where d is the diameter of the particles. We use this structure factor in all our calculations.

In the structure factor, the peak at x_o corresponds to the wavevector $q_o = 2\pi/d_{\text{avg}}$, where d_{avg} is the average center-to-center spacing between nearest neighbors. The peak wavevector q_o gives rise to constructive interference and color, because it sets the relative phase difference between light waves scattered from neighboring particles. Resonant scattering occurs when this phase difference is an integer multiple of 2π. The wavelengths at which this happens can be determined from Eq. (1):

$$\lambda = (4\pi n_{\text{eff}} d/x_o)\sin(\theta/2). \tag{4}$$

To describe the intensity of scattered light that reaches the detector, we integrate the differential scattering cross-section over the solid angle corresponding to the numerical aperture (NA) of our detector, taking into account transmission and refraction at the air-sample interface:

$$\sigma_{\text{detected}} = 1/k^2 \int_{\phi=0}^{2\pi}\int_{\theta_{\min}}^{\pi} T_{s\text{-}a} F S \sin(\theta)\, d\theta\, d\phi, \tag{5}$$

where $T_{s\text{-}a}$ is the Fresnel coefficient for transmission at the sample-air interface, $\theta_{\min} = \pi - \arcsin(\text{NA}/n_p)$ is the minimum scattering angle that we detect, and ϕ is the polar angle in the plane perpendicular to the scattering plane. There is no dependence on ϕ because the particles are spherical and the structure is isotropic.

To compare our calculations to our measurements we now derive a relation between σ_{detected} and the measured reflectivity, R. To do this we must account for extinction of light as it propagates through the sample; the intensity of light scattered from layers close to the surface is higher than the intensity of light scattered deeper in the sample because of attenuation by scattering. Under the assumption of single scattering, this attenuation scales exponentially with depth following Beer's Law, $I(x) = I_o e^{-\rho\sigma x}$, where ρ is the number density of particles, σ is the scattering cross-section for the full solid angle ($0 \leqslant \phi \leqslant 2\pi$, $0 \leqslant \theta \leqslant \pi$), and x is the distance light has propagated in the medium [31]. If the glass consists of slices of infinitesimal thickness δx, the total reflected intensity I is the sum of the intensities δI reflected from each slice: $\delta I = I(x)\sigma_{\text{detected}}\rho\,\delta x$, where σ_{detected} is given by Eq. (5). After integrating both sides and including the Fresnel coefficients for transmission ($T_{a\text{-}s}$) and reflection ($R_{a\text{-}s}$) at the air-sample interface, we find

$$R = T_{a\text{-}s}\frac{\sigma_{\text{detected}}}{\sigma}(1 - e^{-\rho\sigma l}) + R_{a\text{-}s}, \tag{6}$$

where l is the optical thickness of the sample, or the maximum distance that light can propagate in it.

The reflectivity for a glass of PMMA spheres at a volume fraction $\phi = 0.55$, as calculated according to Eq. (6), is shown in Fig. 4. We have omitted the Fresnel coefficient for reflection at the air-sample interface to better illustrate the features that arise from scattering from the bulk colloidal glass. The plot is shown as a function of the scaled particle size kd, where $k = 2\pi n_p/\lambda$. All terms in Eq. (6)—except for the Fresnel reflection coefficient, which adds an offset in amplitude—scale with kd. Thus, this master curve describes reflectivity from a glass made of any particle size (of the same material and

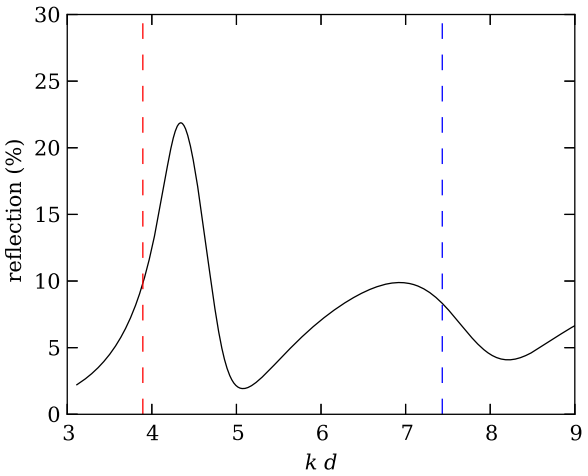

FIG. 4. (Color online) Calculated reflectivity as a function of kd for a photonic glass of spheres at a volume fraction $\phi = 0.55$, as calculated from Eq. (6) with the Fresnel reflection coefficient omitted. The vertical dashed lines denote the kd values that correspond to the range of visible wavelengths we detect, 425 nm (blue line on the right) and 800 nm (red line on the left), when the particle size is $d =$ 334 nm.

volume fraction), assuming dispersion is small. Depending on the particle sizes and refractive indices, different features of the curve will fall within the visible range; here we mark the edges of our detection range for $d = 334$ nm with the blue (425 nm, right) and red (800 nm, left) vertical dashed lines.

IV. RESULTS AND DISCUSSION

The calculated reflectivity reproduces the locations of all of the peaks in our data, as shown in Fig. 5. The only free parameters are the volume fraction $\phi = 0.55$ and the thickness $l = 16\,\mu$m. The peaks predicted by the theory coincide with the peaks in the data for particle diameters $d = 238$ nm [Fig. 5(a)] and $d = 334$ nm [Fig. 5(b)]; these sizes are in good agreement with the sizes of the particles measured with scanning electron microscopy, 240 and 330 nm. The calculated reflectivity for the $d = 334$-nm system also reproduces the peak in the blue that we observe in the data.

The model underestimates the amount of light scattered off-resonance, especially at short wavelengths. We attribute this discrepancy to multiple scattering. Since the probability of multiple scattering increases with the scattering cross-section of individual particles, its contribution should be more pronounced at short wavelengths, which is consistent with what we see.

With this model and data at hand we can address our original question: why does the glass made of 330-nm spheres scatter so much blue light, when we expect the interparticle correlations to give rise only to a resonance in the red? To identify the source of the reflection peaks in this sample, we compare our data to the reflectivities predicted from the form factor alone and, in another comparison, the structure factor alone [Fig. 5(c)]. From the shapes of these two curves we immediately see that the blue peak comes from the form factor and the red peak

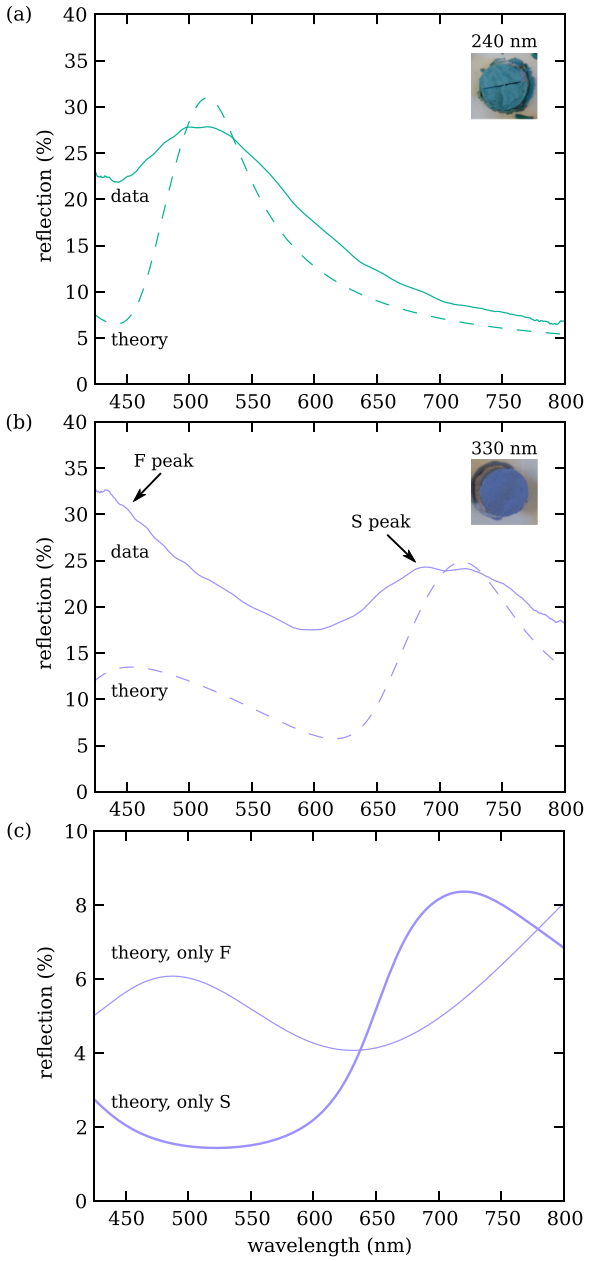

FIG. 5. (Color online) (a, b) Measured (smooth lines) and calculated (dashed lines) reflection spectra of colloidal photonic glasses made of PMMA spheres. Theoretical spectra are calculated from Eq. (6) with $\phi = 0.55$ and $l = 16\ \mu$m. Particle diameters that best fit the measured peaks are 238 nm (a) and 334 nm (b), in good agreement with the measured particle diameters. (c) Calculated reflection spectrum for a photonic glass made from $d = 334$-nm particles, including only the structure factor (thick curve, divided by 10) and only the form factor (thin curve).

from the structure factor, boosted by another peak in the form factor that occurs at a longer wavelength.

We conclude that the structural colors of our photonic glasses are determined not only by interference between waves scattered from correlated particles, but also by resonances in the single-particle scattering cross-section. This can also be seen by rescaling the measured reflectivities by $\sigma_{F,\text{detected}}$ and plotting them as a function of the dimensionless wavevector

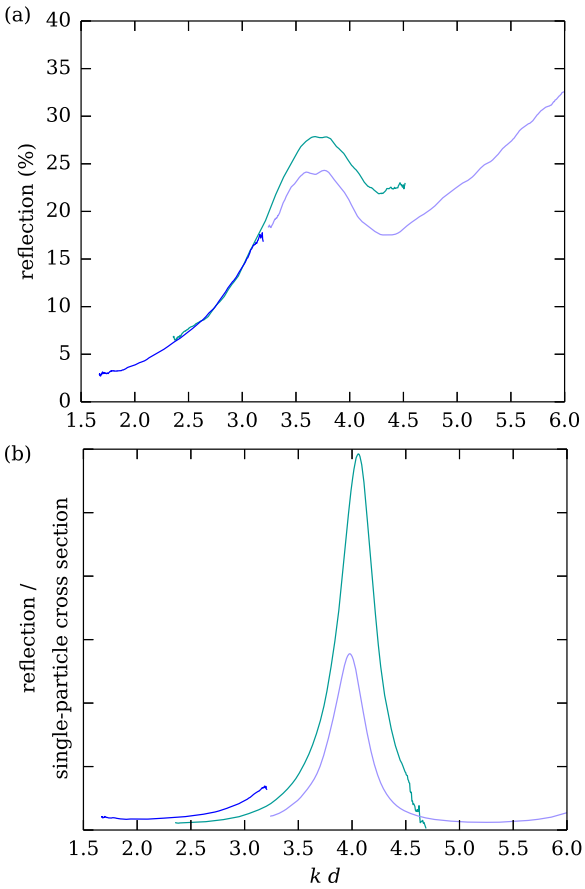

FIG. 6. (Color online) (a) Reflection spectra from Fig. 1 plotted against the dimensionless lengthscale kd. Note the increased scattering at high kd values (short wavelengths) for the $d = 330$-nm sample. (b) Same as (a) but normalized to the single-particle form factor integrated over the detected scattering angles, $\sigma_{F,\text{detected}}$, as defined in Eq. (7). The increased scattering at high kd values disappears, indicating that it is due to the form factor. Differences in amplitude of the peaks are likely due to differences in the sample thickness l.

kd (Fig. 6). Here $\sigma_{F,\text{detected}}$ is the single-particle differential scattering cross-section, integrated over the angle subtended by the detector:

$$\sigma_{F,\text{detected}} = 1/k^2 \int_{\phi=0}^{2\pi} \int_{\theta_{\min}}^{\pi} T_{s\text{-}a} F \sin(\theta)\, d\theta\, d\phi. \qquad (7)$$

We see that after rescaling, the long-wavelength reflectivity peak of the $d = 330$-nm sample coincides with the reflectivity peak of the $d = 240$-nm sample at the same value of kd, showing that these peaks arise from structural resonances, while the short-wavelength (high kd) peak in the $d = 330$-nm sample disappears, showing that it arises from single-particle scattering.

We note that the single-particle resonances responsible for the high reflectivity at small wavelengths are *not* the so-called "Mie resonances." Mie resonances are observed in the *total* single-particle scattering cross-section, obtained by integrating the differential scattering cross-section over all angles. The closest Mie resonance for a 334-nm PMMA particle in our effective medium occurs at 310 nm. Instead, as we shall show,

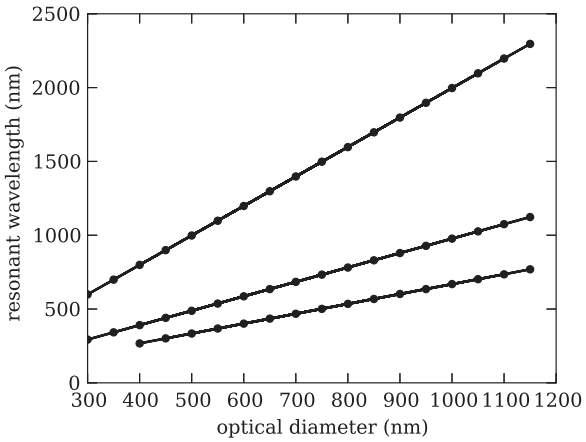

FIG. 7. Resonant wavelengths of the backscattering cross-section, as calculated from Mie theory, as a function of optical diameter $n_p d$ for a refractive index contrast $m = 1.2$, which corresponds to that in our experimental system. The resonant wavelength follows the linear relation $\lambda = 2n_p d/z$ (solid lines), where z is the order of the resonance. Lines correspond to different values of z (top, $z = 1$; middle, $z = 2$; bottom, $z = 3$).

the resonances that contribute to the high reflectivity at small wavelengths occur for scattering angles near backscattering.

We first consider the single-particle scattering cross-section for pure backscattering. This is proportional to the differential scattering cross-section for $\theta = \pi$. As shown in Fig. 7, the backscattering cross-section can have one or more resonances, and the wavelengths at which these occur increase linearly with the particle "optical diameter," $n_p d$, following the relation

$$\lambda_{\text{resonant}} = 2n_p d/z, \qquad (8)$$

where z is an integer that corresponds to the order of the resonance. This suggests that these resonances are akin to those of a Fabry-Pérot cavity, where constructive interference occurs for wavelengths that fit an integer number of times within the round-trip optical pathlength enclosed by the cavity [35]. Similar resonances occur in the differential scattering cross-section for all angles, as shown in Fig. 8. Our calculations show that the resonant wavelength shifts toward the blue as the angle decreases. This blue-shift is consistent with the decrease in the round-trip optical pathlength inside the sphere with decreasing angle (see inset). When the differential scattering cross-section is integrated over the detected solid angle ($\theta = 150°$–$180°$ for our detection numerical aperture of 0.8, after refraction), these resonances, though broadened, persist [Fig. 5(c)]. We therefore conclude that constructive interference of light inside the particles contributes to enhanced reflection at short wavelengths.

Our results show that the absence of red structural color in photonic glasses can be attributed to the blue scattering resonances within the component particles. These resonances occur in addition to the resonances from interparticle correlations, meaning that structural color in photonic glasses arises from the combination of resonant scattering from the structure *and* from the individual particles. For blue and green

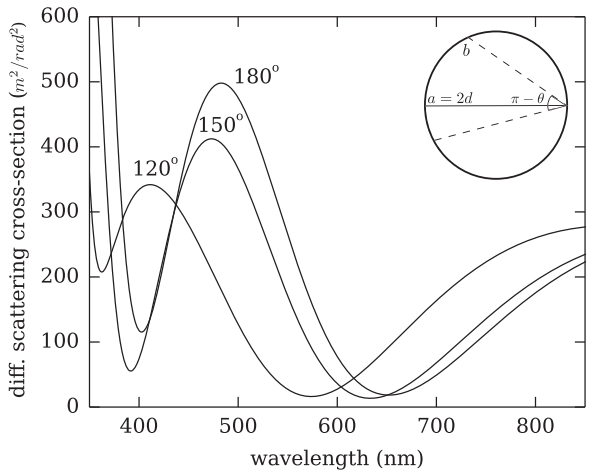

FIG. 8. Single-particle differential scattering cross-sections for various scattering angles as a function of wavelength for a 330-nm PMMA sphere in a colloidal glass of spheres in air at a volume fraction $\phi = 0.55$. The blue-shift in the resonance is consistent with the decrease in optical pathlength inside the sphere with decreasing angle: The longest possible pathlength a is twice the diameter, and $a > b$ for any angle that differs from backscattering.

structural colors, these single-particle scattering resonances do not affect our perception of color because they occur in the UV. While these observations are based on glasses of PMMA spheres, the same principles apply to most typical colloidal materials, such as polystyrene and silica, whose refractive indices are not significantly different from that of PMMA. The chitin particles in beetle scales have similar optical properties [22].

Although the single-particle resonances we observe should also occur in photonic crystals, the structure factor in crystals is much more sharply peaked than in glasses, so that structural resonances can dominate the single-particle resonances, and photonic crystals can have structural red color. The price to be paid for this red color is strong angular dependence: changing the angle between source and detector changes the resonant wavelength, leading to iridescence. Photonic glasses have a lower and broader peak in the structure factor as a consequence of their disorder. The breadth of the peak allows the glass to maintain nearly the same structural color over a range of angles between the source and the detector. At the same time, the low peak amplitude (relative to a crystal) makes the color of the glass susceptible to contamination from the single-particle resonances. Thus, we see that there is an inherent tradeoff between angular independence and structural red color.

Can this tradeoff be broken? One obvious way is to introduce a dye that absorbs blue light. However, this is how traditional colors are produced; red paint, for example, consists of strongly scattering particles mixed with pigment particles that absorb the incident and scattered blue light. In contrast, structural color must arise from resonances that allow scattering at certain wavelengths to dominate scattering at all other wavelengths. The absence of wavelength-dependent absorbers makes structural color appealing for applications such as coatings, because all colors can be produced from the same materials. Therefore, we pursue a different way to break the tradeoff between angular independence and long-wavelength structural color.

To create a red structural color, we would need to manipulate the resonances from two independent processes: single-particle scattering and coherent scattering from the particle assembly. The characteristic scale for the single-particle scattering resonances is the particle optical diameter $n_p d$ [Eq. (8)], and for the structural resonances it is the effective interparticle spacing $n_{\text{eff}} d_{\text{avg}}$ [Eq. (4)]. Our control parameters are therefore the particle diameter d, its refractive index n_p, the interparticle spacing d_{avg}, and the index of the medium n_{med}, which determines the effective index n_{eff}.

Red photonic glasses could be made by tuning these control parameters to blue-shift the second resonance of the form factor into the UV while keeping the peak of the structure factor at long wavelengths. This can be achieved with particles that have a small optical diameter, as shown in Fig. 7. The simplest way to reduce the optical diameter is to use particles with a refractive index smaller than that of the medium. In these *inverse* glasses, the diameter of the particles is about the same as the spacing between their centers ($d_{\text{avg}} \sim \sqrt{6}d/3$), but their lower refractive index makes the optical pathlength inside each particle shorter than the optical pathlength between two particles. As a result, the form factor resonances are blue-shifted compared to those of our PMMA colloids of similar size, while the structure factor resonances remain at about the same wavelength.

Another effective way to blue-shift the form factor resonance while not shifting the structural resonance is to decouple the particle size from the interparticle spacing and to use smaller particles as the scatterers. This can be done by packing core-shell particles with a strongly scattering core and a transparent shell. We have already demonstrated that this approach enables the creation of full-spectrum, angle-independent structural pigments [21]. Such pigments still suffer from poor color saturation in the red compared to the blue, but the short-wavelength reflectivity is substantially reduced relative to colloidal glasses made of homogeneous (that is, not core-shell) particles.

One can combine the core-shell and inverse-structure approaches to design a system with a single visible resonance at long wavelengths. In particular, the shell diameter could be chosen such that the interparticle spacing gives rise to a resonance in the red, and the core diameter chosen such that the first-order peak in the form factor boosts the peak from the structure factor, while the second-order form-factor peak is fully in the ultraviolet. Our calculations show that such a structure could be made from core-shell particles with air cores and silica shells, embedded in a silica matrix, as shown in Fig. 9.

Curiously, the photonic structures found in bird feathers resemble these inverse glasses: they often consist of air pockets in a matrix of β-keratin [9,11] that has a refractive index close to that of silica [36]. However, birds do not seem to have taken advantage of their inverse structures for colors other than blue. They rely instead on pigments to acquire yellow, orange, and red colors [11,37]. Whether this is due to a physical effect not accounted for in our model or is the result of evolution or chance remains to be seen.

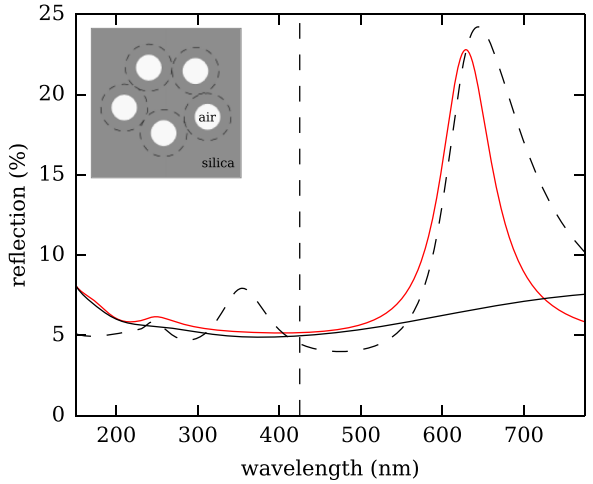

FIG. 9. (Color online) Calculated reflection for an inverse glass of core-shell spheres engineered to scatter most strongly in the red. The continuous red curve with the peak at 632 nm includes both the structure and the form factor, the dashed black curve only the structure factor (divided by 2), and the black continuous curve only the form factor. The vertical dashed line marks 425 nm, the low-wavelength limit in our spectral measurements. The optimal design has air cores with diameter 260 nm and silica shells with diameter 280 nm, and the particles are embedded in a silica matrix. The reflectivity peak at 632 nm is primarily due to the structure factor and determined by the shell diameter. One form-factor resonance occurs in the near-IR, boosting the structural resonance in the red, and another occurs deep in the UV (at about 150 nm), too far away from the visible regime to affect the color.

V. CONCLUSIONS

We have described a physical mechanism that explains the scarcity of angle-independent structural red color in photonic glasses. Our model shows that interparticle correlations alone are not sufficient to understand the reflectivity of photonic glasses. The scattering behavior of their constituent particles plays an equally important—and previously unrecognized—role. In particular, interference of light *inside* the particles can lead to enhanced scattering at wavelengths other than those related to the interparticle correlations. Our model describes our experimental observations well, and it can be used to guide the design of new photonic glasses with purely red structural color.

To this end, we have shown that it is possible to control the locations of both the single-particle scattering resonances and the structural resonances by tuning the refractive indices, particle sizes, and interparticle distances. Our model predicts that inverse glasses made of core-shell particles with a low-index core and a high-index shell that is index-matched to the medium might produce angle-independent structural red color. If future experiments show that such structures show poor color saturation in the red, these results would suggest that another mechanism, such as multiple scattering, should be accounted for. If successful, these structures would complete the palette of visible colors achievable with photonic glasses, opening the path to their use in practical applications such as long-lasting dyes or reflective displays.

ACKNOWLEDGMENTS

We thank W. Benjamin Rogers, Max Lavrentovich, Zorana Zeravcic, Jason Forster, and Eric Dufresne for helpful discussions and Rodrigo Guerra for the PMMA particles. This work was supported by an International Collaboration Grant (Grant No. Sunjin-2010-002) from the Korean Ministry of Trade, Industry & Energy of Korea and by the Harvard MRSEC (NSF Grant No. DMR-0820484). It was performed in part at the Center for Nanoscale Systems (CNS), a part of Harvard University and a member of the National Nanotechnology Infrastructure Network (NNIN), which is supported by NSF Grant No. ECS-0335765.

[1] J. Sanders, Nature **204**, 1151 (1964).
[2] F. Marlow, Muldarisnur, P. Sharifi, R. Brinkmann, and C. Mendive, Angewandte Chemie Int. Ed. **48**, 6212 (2009).
[3] J. D. Joannopoulos, S. G. Johnson, J. N. Winn, and R. D. Meade, *Photonic Crystals: Molding the Flow of Light*, 2nd ed. (Princeton University Press, Princeton, NJ, 2008).
[4] J. Ballato, J. Opt. Soc. Am. B **17**, 219 (2000).
[5] L. F. Rojas-Ochoa, J. M. Mendez-Alcaraz, J. J. Sáenz, P. Schurtenberger, and F. Scheffold, Phys. Rev. Lett. **93**, 073903 (2004).
[6] P. García, R. Sapienza, A. Blanco, and C. López, Adv. Mater. **19**, 2597 (2007).
[7] P. D. García, R. Sapienza, and C. López, Adv. Mater. **22**, 12 (2010).
[8] J. D. Forster, H. Noh, S. F. Liew, V. Saranathan, C. F. Schreck, L. Yang, J.-G. Park, R. O. Prum, S. G. J. Mochrie, C. S. O'Hern, H. Cao, and E. R. Dufresne, Adv. Mater. **22**, 2939 (2010).
[9] H. Noh, S. F. Liew, V. Saranathan, S. G. J. Mochrie, R. O. Prum, E. R. Dufresne, and H. Cao, Adv. Mater. **22**, 2871 (2010).
[10] R. O. Prum, R. H. Torres, S. Williamson, and J. Dyck, Nature **396**, 28 (1998).
[11] V. Saranathan, J. D. Forster, H. Noh, S.-F. Liew, S. G. J. Mochrie, H. Cao, E. R. Dufresne, and R. O. Prum, J. Roy. Soc. Interf. **9**, 2563 (2012).
[12] Y. Takeoka, M. Honda, T. Seki, M. Ishii, and H. Nakamura, ACS Appl. Mater. Interf. **1**, 982 (2009).
[13] K. Ueno, A. Inaba, Y. Sano, M. Kondoh, and M. Watanabe, Chem. Commun. 3603 (2009).
[14] K. Ueno, Y. Sano, A. Inaba, M. Kondoh, and M. Watanabe, J. Phys. Chem. B **114**, 13095 (2010).
[15] M. Harun-Ur-Rashid, A. Bin Imran, T. Seki, M. Ishii, H. Nakamura, and Y. Takeoka, Chem. Phys. Chem. **11**, 579 (2010).
[16] I. Lee, D. Kim, J. Kal, H. Baek, D. Kwak, D. Go, E. Kim, C. Kang, J. Chung, Y. Jang, S. Ji, J. Joo, and Y. Kang, Adv. Mater. **22**, 4973 (2010).
[17] N. Kumano, T. Seki, M. Ishii, H. Nakamura, and Y. Takeoka, Angew. Chem. Int. Ed. **50**, 4012 (2011).

[18] Y. Gotoh, H. Suzuki, N. Kumano, T. Seki, K. Katagiri, and Y. Takeoka, New J. Chem. **36**, 2171 (2012).
[19] S. Magkiriadou, J.-G. Park, Y.-S. Kim, and V. N. Manoharan, Opt. Mater. Express **2**, 1343 (2012).
[20] Y. Takeoka, S. Yoshioka, A. Takano, S. Arai, K. Nueangnoraj, H. Nishihara, M. Teshima, Y. Ohtsuka, and T. Seki, Angewandte Chemie Int. Ed. **52**, 7261 (2013).
[21] J.-G. Park, S.-H. Kim, S. Magkiriadou, T. M. Choi, Y.-S. Kim, and V. N. Manoharan, Angewandte Chemie **126**, 2943 (2014).
[22] B. Q. Dong, X. H. Liu, T. R. Zhan, L. P. Jiang, H. W. Yin, F. Liu, and J. Zi, Opt. Express **18**, 14430 (2010).
[23] S. F. Liew, J.-K. Yang, H. Noh, C. F. Schreck, E. R. Dufresne, C. S. O'Hern, and H. Cao, Phys. Rev. A **84**, 063818 (2011).
[24] L. D'Alba, V. Saranathan, J. A. Clarke, J. A. Vinther, R. O. Prum, and M. D. Shawkey, Biol. Lett. **7**, 543 (2011).
[25] E. R. Dufresne, H. Noh, V. Saranathan, S. G. J. Mochrie, H. Cao, and R. O. Prum, Soft Matter **5**, 1792 (2009).
[26] H. Noh, S. F. Liew, V. Saranathan, R. O. Prum, S. G. J. Mochrie, E. R. Dufresne, and H. Cao, Opt. Express **18**, 11942 (2010).
[27] H. Noh, S. F. Liew, V. Saranathan, R. O. Prum, S. G. J. Mochrie, E. R. Dufresne, and H. Cao, Phys. Rev. E **81**, 051923 (2010).
[28] P. D. Kaplan, A. D. Dinsmore, A. G. Yodh, and D. J. Pine, Phys. Rev. E **50**, 4827 (1994).
[29] J. C. Maxwell Garnett, Phil. Trans. R. Soc. Lond. A **203**, 385 (1904).
[30] W. L. Vos, R. Sprik, A. van Blaaderen, A. Imhof, A. Lagendijk, and G. H. Wegdam, Phys. Rev. B **53**, 16231 (1996).
[31] C. F. Bohren and D. R. Huffman, *Absorption and Scattering of Light by Small Particles* (Wiley-VCH Verlag GmbH, Berlin, 2004).
[32] G. Mie, Ann. Physik **330**, 377 (1908).
[33] P. M. Chaikin and T. C. Lubensky, *Principles of Condensed Matter Physics* (Cambridge University Press, Cambridge, 2007).
[34] J. K. Percus and G. J. Yevick, Phys. Rev. **110**, 1 (1958).
[35] E. Hecht, *Optics* (Addison-Wesley, Boston, 2002).
[36] H. L. Leertouwer, B. D. Wilts, and D. G. Stavenga, Opt. Express **19**, 24061 (2011).
[37] M. C. Stoddard and R. O. Prum, Behav. Ecol. **22**, 1042 (2011).